Influence of dipolar energy on the magnetization reversal in magnetization-modulated thin film systems: Model and experiment

Norbert Martin,[1,*] Ingolf Mönch,[2] Rudolf Schäfer,[2,3] Jürgen Fassbender,[1] Ludwig Schultz,[2,3] and Jeffrey McCord[1]

[1]*Institute of Ion Beam Physics and Materials Research, Helmholtz-Zentrum Dresden Rossendorf e.V., P.O. Box 510119, D-01314 Dresden, Germany*

[2]*Leibniz Institute for Solid State and Materials Research IFW Dresden, P.O. Box 270116, D-01171 Dresden, Germany*

[3]*Department of Mechanical Engineering, Institute for Materials Science, TU Dresden, D-01062 Dresden, Germany*

(Received 27 January 2011; revised manuscript received 10 March 2011; published 10 May 2011)

Laterally patterned magnetic hybrid structures display novel magnetic reversal properties, which are related to the fundamental exchange coupling between material interfaces. We present an analytical model that depicts the influence of dipolar fields in mesoscopic structures with modulated saturation magnetization on the magnetization reversal and the local magnetic states, as well as the occurrence of a lateral exchange-spring effect. This is done by confining a lateral array of stripes with alternating saturation magnetization M_S in a micrometer-sized square, introducing external boundary conditions to the system. The calculations were performed for distinct stripe and array sizes, as well as different M_S values. From the calculations a stability region of array and stripe sizes is derived, in which the lateral exchange-spring effect occurs. The obtained modeling results were found to be in agreement with the experimental data. The model adds a building block to the fundamental understanding of magnetic hybrid structures.

DOI: 10.1103/PhysRevB.83.174423 PACS number(s): 75.70.Cn

I. INTRODUCTION

The influence of lateral patterning on the magnetization configuration of thin films is of fundamental interest in the field of micromagnetism and magnonic crystals.[1–3] One major aspect of the research is the characterization of the interplay between dipolar interactions in finite samples, the exchange coupling, and external magnetic fields.[4] Several studies have been performed to simulate the influence of this interplay on the magnetization reversal, numerically by finite difference or finite element methods.[5,6] These calculations are, however, very time consuming for systems larger than several micrometers, since a quantitatively correct evaluation requires cell sizes on the order of the exchange length, which is in general in the lower nanometer regime. One alternative route is to calculate magnetization configurations analytically, which has been performed already with good agreement to experimental results for a lot of standardized cases like, e.g., ellipsoids and extended thin films.[7,8] Yet very few calculations have been performed on laterally exchange coupled structures with periodically changing magnetic properties like saturation magnetization M_S and magnetic anisotropy.[9] One interesting effect that is observable in such structures is the lateral exchange-spring effect between magnetically hard and soft stripes.[10] This effect is based on the formation of domain walls between the stripes, when the magnetization in the soft stripes is switched upon the application of an external magnetic field. As in a regular multilayered exchange-spring system, the soft stripes align back into the orientation of the hard stripes after removal of the magnetic field.[11] This is, however, not the whole story for a confined stripe array in which parallel-aligned magnetizations in the stripes point perpendicularly to an external boundary and therefore the dipolar energy has to be taken into account.

In this paper an analytical model is presented from which the influence of dipolar energy on the lateral exchange-spring effect in confined arrays of M_S-modulated stripe structures is calculated. The model results are compared to experimental data. The samples used for the comparison were fabricated by means of local ion implantation into ferromagnetic thin films.[9] By this, the saturation magnetization of $Ni_{81}Fe_{19}$ can be tailored very accurately by implanting different doses of chromium.[12] Therefore it is possible to experimentally compare the model with different sample parameters and thus to prove the model's reliability.

II. SAMPLE PREPARATION

$Ni_{81}Fe_{19}$ (20 nm) films were deposited by means of dc-magnetron sputtering onto an oxidized silicon wafer with a 5-nm Ta seed layer to promote a ⟨111⟩ crystallographic texture and thereby optimal soft-magnetic properties. The deposition parameters can be found elsewhere.[10] After the deposition the $Ni_{81}Fe_{19}$ film was patterned into a stripe array of modulated saturation magnetization via photolithography and subsequent irradiation with Cr ions at an ion energy of $E = 30$ keV. The width of the stripes was set between 1 and 4 μm. The simulated radial distribution of the chromium is 7 nm.[13] According to this, the lateral size of the interface between the stripes can be considered as very small compared to the stripe width. The fluence was chosen to set ratios of $M_{SL}/M_{SH} = 0.8, 0.5$, and 0.2, which correspond to irradiation fluences of 2.0×10^{15}, 7.7×10^{15}, and 1.5×10^{16} cm^{-2}. Here M_{SL} and M_{SH} represent low and high values, respectively, of the saturation magnetization. The ratio $M_{SL}/M_{SH} = 0$, the case of isolated, regularly structured stripes, was prepared by e-beam lithography and subsequent Ar etching of the unmasked stripes.

III. MODELING OF THE $M(H)$ BEHAVIOR

The considered model system consists of a stripe array with lateral dimensions of $L \times L$, as sketched in Fig. 1. The

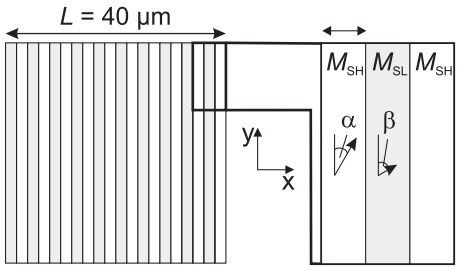

FIG. 1. Schematic view of the model system of a stripe array with alternating M_S, where $M_{SH} \geqslant M_{SL}$. α and β represent the angles of magnetization in the two types of stripe.

lateral dimensions are set to $40 \times 40\,\mu\text{m}^2$. The width of the stripes varies between $w = 1$ and 20 μm, while the stripe width within one array remains constant. The difference in the magnetic properties of the stripes is the value of the saturation magnetization M_S, being high M_{SH} or low M_{SH}, meaning $M_{SH} \geqslant M_{SL}$. The value of M_{SH} for the calculations is $M_{SH} = 800\,\text{kA m}^{-1}$. We treat the system as a serial connection of magnetic volumes with different M_S values along the x axis and a parallel connection along the y axis. The ratio of M_{SL}/M_{SH} is varied between zero (isolated stripes) and 1 (homogenous magnetic properties). α and β are the directions of magnetization within the high- and low-moment stripes, respectively.

For the model we describe the energy density of the ferromagnetic thin film system e_{tot},

$$e_{tot} = e_{ex} + e_d + e_{Zee}, \tag{1}$$

as a sum of three energy densities, namely, the exchange e_{ex}, the dipolar e_d, and the magnetic-field energy density e_{Zee}.[14] The low magnetic anisotropy energy of the soft magnetic film is neglected. The magnetization is assumed to be homogeneous within each of the stripes. Therefore possible exchange-energy terms only originate at the interfaces between the individual stripes, i.e. inside the magnetic domain walls. The energy of a domain wall depends on the thickness of the film t, the wall length L, and the angle between the magnetization components on both sides of a wall. For Néel walls[15] the specific energy can be estimated using the following equation:[16,17]

$$\gamma_{wall} = \gamma_0 \left[1 - \cos\left(\frac{\alpha - \beta}{2}\right)\right]^2. \tag{2}$$

In the equation γ_0 is the specific energy of a 180° wall that scales with the saturation magnetization and the exchange constant of the ferromagnet.[18] Accordingly, the walls are preferably located in the stripes with lower saturation magnetization M_{SL} in order to reduce the domain-wall energy.

The Zeeman or field energy depends on M_S and the direction of magnetization in the individual stripes and the angle between the external field H_{ext}. It is calculated by

$$e_{Zee} = -\mu_0 \frac{L}{2w}(\vec{H}_{ext} \cdot \vec{M}_{SH} + \vec{H}_{ext} \cdot \vec{M}_{SL}). \tag{3}$$

The ratio $L/2w$ determines the number of both the M_{SH} and the M_{SL} stripes, assuming an equal width of both stripe types.

The dipolar energy density e_d originates from a discontinuous magnetic flux transport via $\vec{M}$ due to different magnetization components along the interfaces. The relation between the magnetization of a ferromagnet and the magnetic flux Φ is generally described by the fundamental equation $\Phi = \int_A \vec{B} \cdot d\vec{A}$, where $\vec{B} = \mu_0(\vec{H}_{ext} + \vec{M}_S)$ is the flux density and $\vec{A}$ is the normal vector to the interface area. One obvious outcome of this relation is the reduced capability of the M_{SL} stripes to transport flux via the magnetization $\vec{M}$ as compared to the M_{SH} stripes. Therefore a discontinuous flux transport via M can occur at all of the interfaces present in the model system, which will contribute to e_d. In the system of interest these interfaces are the internal interfaces M_{SH}-M_{SL} and the external boundaries given by the lateral dimensions of the stripe array. In order to evaluate e_d for any magnetization configuration in the xy plane, the overall magnetization configuration of the system is split into partial configurations, for which the dipolar energies are calculated. This is sketched in Fig. 2. For parallel-aligned magnetization components [Fig. 2(a)], the system is split into (a1) a square with the length L and $\vec{M} = \vec{M}_{SL}$ and (a2) isolated stripes with $\Delta\vec{M} = \vec{M}_{SH} - \vec{M}_{SL}$. The dipolar energy $e_{d,a1}$ of the square shown in Fig. 2(a1) can be calculated by

$$e_{d,a1} = \tfrac{1}{2}\mu_0 N_{SQ} \vec{M}^2 = \tfrac{1}{2}\mu_0 N_{SQ} M_{SL}^2. \tag{4}$$

The demagnetizing factor N_{SQ} for a square with a size of the stripe array and all other further demagnetizing factors are calculated by the ansatz of Aharoni for effective demagnetizing factors of prisms.[19] The partial configuration displayed in Fig. 2(a2) has to be considered due to the additional component to the dipolar energy that originates from the higher M_S of the M_{SH} stripes:

$$e_{d,a2} = \frac{1}{2}\mu_0 N_{STx} \frac{L}{2w}(M_{SH}\sin\alpha - M_{SL}\sin\beta)^2 + \frac{1}{2}\mu_0 N_{STy} \frac{L}{2w}(M_{SH}\cos\alpha - M_{SL}\cos\beta)^2 \tag{5}$$

with N_{STx} and N_{STy} being the demagnetizing factors along x and y for a prism with the same size as an individual stripe.

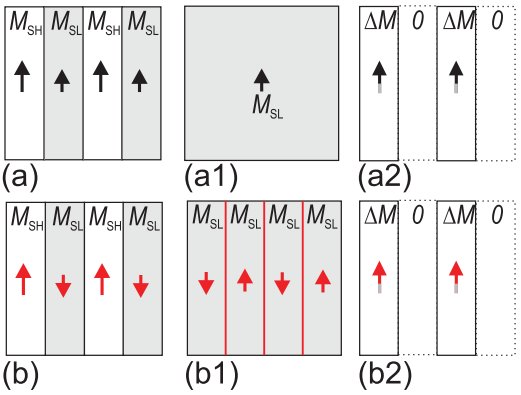

FIG. 2. (Color online) Splitting of possible magnetization states into configurations that are calculated. For parallel-aligned magnetizations (a) the contributions to the energy are the dipolar energy of a saturated square with M_{SL} (a1) and the dipolar energy of stripes with $\Delta M = M_{SH} - M_{SL}$ (a2). In the antiparallel configuration (b), the dipolar energy is split into contributions from a uniaxial domain pattern with alternating saturation magnetization M_{SL} and (b1) the dipolar energy of stripes with $\Delta M = M_{SH} - M_{SL}$ (b2).

The other magnetization configuration of interest is the case of antiparallel magnetized stripes ($|\alpha - \beta| > \frac{\pi}{2}$) as depicted by the red arrows in Fig. 2(b). In order to calculate the dipolar energy of this configuration, e_d is divided into an array with antiparallel aligned domains and the magnetization $M = M_{SL} \cos\beta$ as in Fig. 2(b1). Analytical expressions, which can be applied to the presented partial magnetization configurations in Fig. 2(b1), can be found in the literature,[20,21] which lead to the description of the dipolar energy $e_{d,b1}$:

$$e_{d,b1} = \frac{1}{2}\mu_0 N_{SQ}(M_{SL}\cos\beta)^2 \frac{8w}{\pi^3 L}\sum_{n=1}^{\infty} n^{-3}\sin^2\left(\frac{\pi}{2}n\right) \times\left[1+\exp\left(-\pi n\frac{L}{w}\right)\right]. \quad (6)$$

This equation calculates the dipolar energy for an extended stripe pattern. The deviation from the proposed model, which consists of 10–40 stripes, is, however, rather low since the dipolar interactions between the stripes reduce with distance cubed. According to this, the existence of the side edges parallel to the stripes influences mostly the stripes directly located at the edge and the influence on the overall behavior can be neglected. The additional component to the dipolar energy, originating from $M_{SH} > M_{SL}$, is calculated using Eq. (5).

In order to determine the stability of the lateral exchange-spring behavior dependent on $\mu_0\vec{H}_{ext}$, L, and w, the total energy e_{tot} is minimized with respect to $\vec{M}_{SL}$ and $\vec{M}_{SH}$. Exemplary calculated magnetic reversal loops for stripe widths of $w = 1$ and $2\,\mu$m and a ratio $M_{SL}/M_{SH} = 0.5$ are plotted in Fig. 3(a). One result of this calculation is the equilibrium magnetization configuration at zero external field [see Fig. 3 sketch (1)], in which the magnetization, in all stripes, points parallel to the stripe axis along the same direction. This is the stable configuration as the domain-wall energy of the antiparallel alignment of magnetization is larger than the dipolar energy contribution for the parallel alignment. When increasing the field, which is oriented perpendicular to the stripe axis, in the magnetization loop two regions of high and low permeability become visible. The difference in permeability can be explained by analyzing the magnetization components of the individual stripes, as plotted in Figs. 3(b) and 3(c): The magnetization in the M_{SL} stripes saturates along the x axis at small applied fields and $M_{SH}\sin\alpha = M_{SL}\sin\beta$. For magnetic fields above the saturation field of the M_{SL} stripes the magnetization M_{SH} starts to rotate in the direction of the external field until it is finally saturated at $\mu_0 H_S = \pm 16$ mT. Both the equal components of magnetization $M_{SH}\sin\alpha = M_{SL}\sin\beta$ below $\mu_0 H = 1$ mT and the high saturation fields $\mu_0 H = 16$ mT for the M_{SH} stripes originate from the additional dipolar energy that results from the discontinuity of M across the interfaces, as defined before in Eq. (5). For magnetic fields above 1 mT the additional dipolar energy acts as an effective uniaxial shape anisotropy K_u in the M_{SH} stripes. The overall magnetization process is reversible. The strength of K_u and therefore the saturation field $\mu_0 H_S$ depend on the ratio M_{SL}/M_{SH} and the width of the M_{SH} stripes. The calculated dependency is plotted in Fig. 4. With increasing ratio of $0 \leqslant M_{SL}/M_{SH} \leqslant 1$ the dependence of the saturation field on the stripe width decreases. This is attributed to a lower discontinuity of flux transport along the internal interface and thus a lower effective anisotropy K_u.

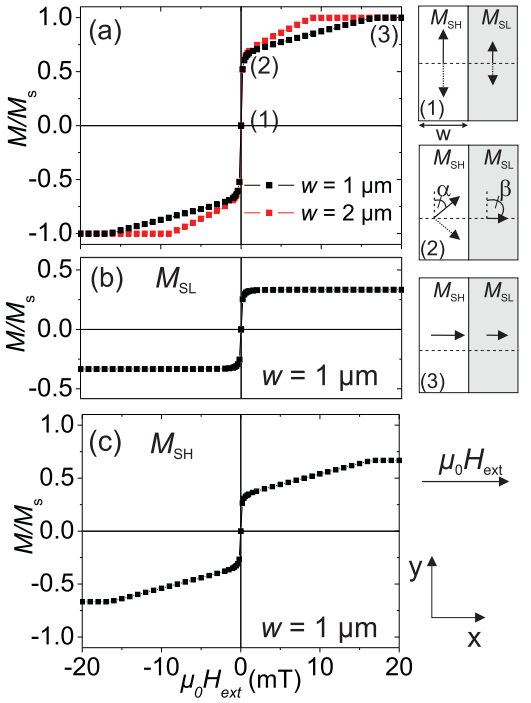

FIG. 3. (Color online) (a) Analytically calculated hysteresis curves for stripe widths of 1 and 2 μm and $M_{SL}/M_{SH} = 0.5$. In (1) and (2) the possible magnetization configurations within each stripe are sketched. The straight arrows represent the alignment of the magnetization at zero field and the dashed arrows represent a state of equal energy. (b),(c) Magnetization loops calculated for the individual stripes.

The values of M_{SL}/M_{SH} and w also influence reversal curves with $\mu_0 H$ parallel to the stripe axis. Exemplary hysteresis curves, calculated for $w = 1$ and $2\,\mu$m at a ratio $M_{SL}/M_{SH} = 0.5$, show two switching processes [see Fig. 5(a)]. The first process corresponds mostly to the switching of the M_{SL} stripes at external fields close to zero. This becomes visible from the individual magnetization components, which are plotted in Figs. 5(b) and 5(c). There is also a small step visible in the M_{SH} curve in Fig. 5(c), which is attributed to the formation of low-angle domain walls due to the interaction of the neighboring stripes. For higher external

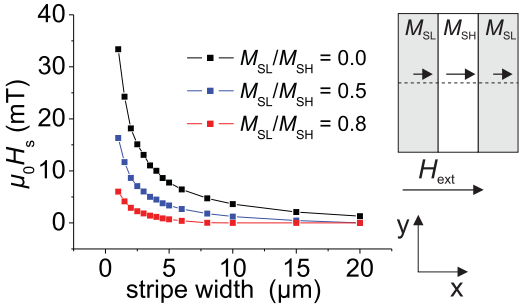

FIG. 4. (Color online) The external field $\mu_0 H_S$ necessary to saturate the stripe array vs the stripe width at three different ratios of M_{SL}/M_{SH}.

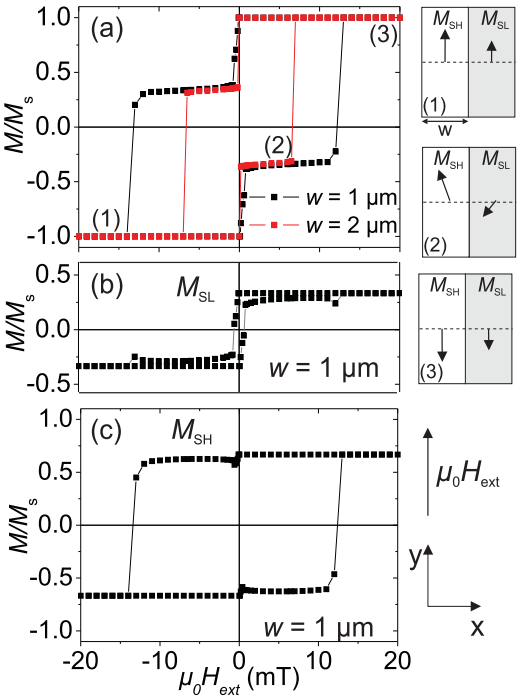

FIG. 5. (Color online) (a) Analytically calculated hysteresis curves for stripe widths of 1 and 2 μm and $M_{SL}/M_{SH} = 0.5$. The external field is aligned parallel to the y direction. The sketches (1), (2), and (3) show the magnetization configuration within each stripe. In (b) and (c) the magnetization reversal loops of the individual stripes are displayed.

fields the Zeeman energy becomes dominant and finally $\vec{M}_{SH}$ switches in the direction of the external field. The switching process at $\mu_0 H_{1\mu m} = 12$ mT corresponds to the magnetization reversal of the M_{SH} stripes by Stoner-Wohlfarth switching, which represents the upper limit of the magnetic switching field.[22,23] The switching field of the array with $w = 2$ μm is lowered due to the smaller aspect ratio L/w and therefore lower effective K_u. The general dependence of L/w and M_{SL}/M_{SH} on the stability of the described reversal process is plotted in Fig. 6. It shows that the two-step reversal with the homogeneous zero-field magnetization configuration is stable over a wide range of M_{SL}/M_{SH} values, if the aspect ratio L/w is large. High values of $L/w \gg 1$ occur at large array sizes and/or small stripe widths. In this case the shape anisotropy dominates the effective anisotropy. Therefore K_u is large over a wide range of M_{SL}/M_{SH} values, thus stabilizing a parallel magnetization, which is a necessary precondition for the formation of the exchange-spring behavior. Smaller aspect ratios $L/w > 1$ result in a reduced shape anisotropy contribution and the parallel alignment of magnetization is only stable for $M_{SL}/M_{SH} \to 0$, by which the effective anisotropy increases.

The analytical model, and with this the phase diagram in Fig. 6, is valid only for values of the stripe length and width larger than the characteristic length scales of a Néel-wall core $L_{core} \approx 70$ nm, which is fulfilled for the shown dimensions.[24,25] Otherwise the magnetic properties are dominated by exchange coupling and no domain walls form.[26] The experimental evaluation of the fundamental effects

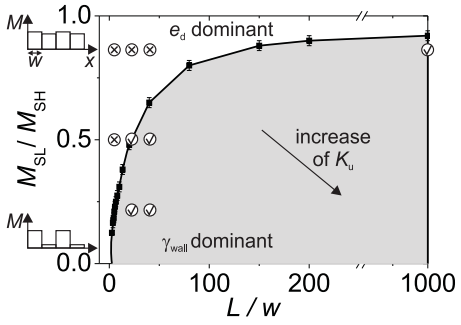

FIG. 6. Phase diagram showing the transition between magnetization reversal governed by the internal interfaces or by the external boundaries. The stability of each phase depends on the ratio of the stripe length L to the stripe width w and the ratio M_{SL}/M_{SH}. The dots mark experimental data regarding the occurrence of the exchange-spring behavior. The measurement data for $L/w = 1000$ are taken from Ref. 10.

calculated by the presented model is shown in the next section.

IV. COMPARISON OF MODEL AND EXPERIMENT

The magnetic hysteresis loops and the magnetization configuration of the samples were analyzed by means of high-resolution magneto-optical Kerr effect microscopy in the longitudinal mode.[27] The magnetization loops and the corresponding magnetic domain images were measured parallel and perpendicular to the stripes for all experimentally fabricated stripe widths and ratios M_{SL}/M_{SH}. The analysis of the reversal behavior shows good agreement with the calculations. The measured and calculated magnetization reversal curves for $\mu_0 H_{ext}$ perpendicular to the stripes for an array with $L = 40$ μm, $w = 1$ μm, and $M_{SL}/M_{SH} = 0.5$ are shown in Fig. 7. The proposed model accurately predicts the magnetization reversal process for the analyzed sample. The main difference is the saturation field, which is slightly smaller in the experiment. One reason for this is a lower effective demagnetizing field in the center of the stripes as compared to the edge regions, resulting in an inhomogeneous magnetization distribution.[28] The magnetization reversal for $\mu_0 H$ parallel to the stripes and the corresponding magnetization images are plotted in Fig. 8. A lateral exchange-spring effect is found in both simulation and experiment (see inset in Fig. 8).

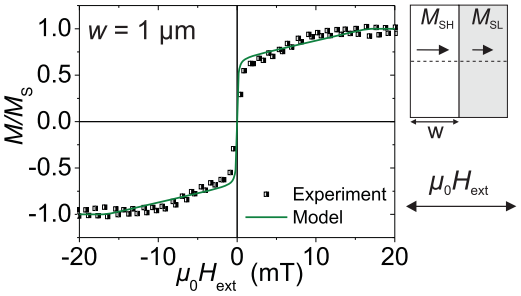

FIG. 7. (Color online) Magneto-optically measured magnetization reversal curve of a sample with $M_{SL}/M_{SH} = 0.5$ and $w = 1$ μm. The corresponding calculated loop from Fig. 3 is added for comparison.

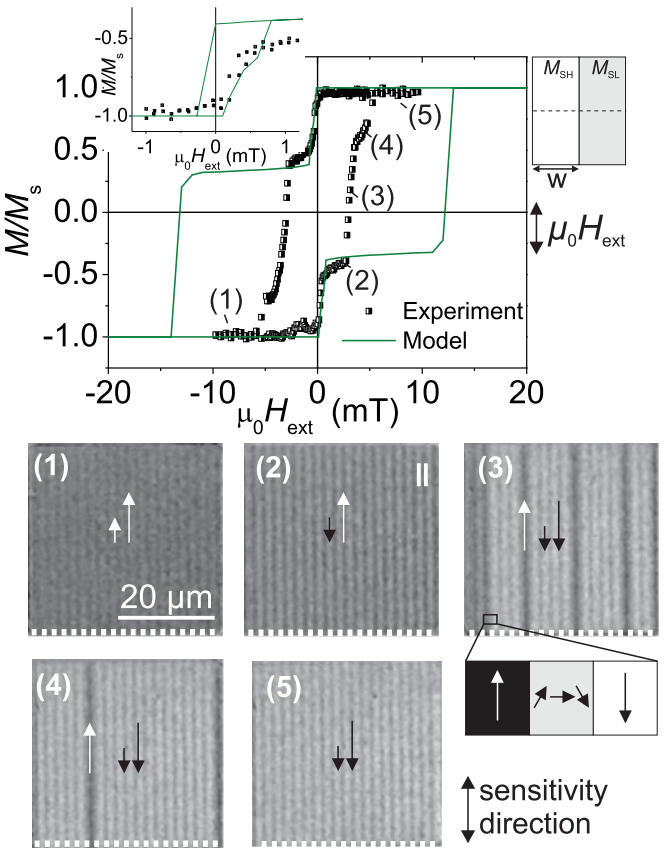

FIG. 8. (Color online) Magneto-optically measured hysteresis curve of a sample with $M_{SL}/M_{SH} = 0.5$ and $w = 1\,\mu$m with corresponding magnetization images. The inset is the corresponding minor loop. The modeled magnetization reversal behavior is added for comparison in both loops. The corresponding magnetic domain images are shown underneath.

As predicted by the model, the experimentally observed exchange-spring behavior occurs only for samples in which the internal interfaces govern the magnetization reversal process (see marks in Fig. 6). Differences between calculation and experiment for H_{ext} parallel to the stripes are visible for the second reversal process and the saturation field.

In the calculated hysteresis loop, the magnetization saturates at a certain threshold field, while a wide switching field distribution is visible in the experimental data. Magneto-optical domain analysis explains this deviation. In the experiment the magnetization in the stripes reverses individually, distributed over a field range of around 3 mT, while in the model a collective switching of all stripes is assumed. The partially switched magnetization configurations in Figs. 8(3) and 8(4) also introduce domain walls as depicted by the sketch below (3). The domain wall is located in the middle of the stripe and M varies over the whole stripe width. Such a case occurs for partial switching only and is not considered in the model. The model calculates the switching field, when M in all stripes reverses by coherent rotation. The reversal mechanism in the experiment is via nucleation and propagation of a domain wall, which can be simulated numerically.[5] However, one has to check carefully which reversal mechanism takes place, since it is well known that coherent rotation is independent

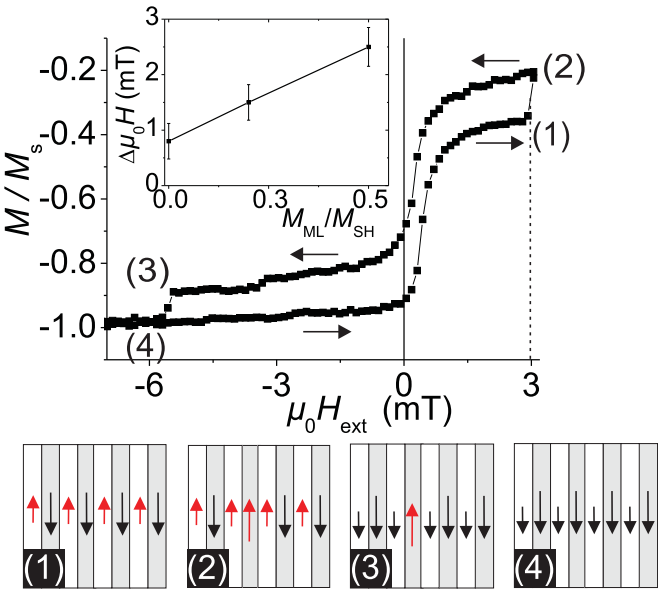

FIG. 9. (Color online) Minor loop behavior of a stripe array with stripe width $w = 1\,\mu$m and the ratio $M_{SL}/M_{SH} = 0.5$. The magnetization configurations of the states of magnetization 1–4 are sketched below the graph. The inset shows the difference between the absolute switching fields $\mu_0 H_{1-2}$ and $\mu_0 H_{3-4}$.

of any nucleation phenomena and always represents the upper limit of the switching field. For different partially antiparallel magnetic configurations, however, different switching fields are expected. Minor hysteresis loops, as shown in Fig. 9, are measured to clarify the origin of the switching distribution. The corresponding magnetization configurations for the measured loop are roughly sketched in Fig. 9. It demonstrates that the difference between $\mu_0 H_{1-2}$ and $\mu_0 H_{3-4}$ is caused by a stronger increase in dipolar energy for the transition "3-4" than for transition "1-2" due to the change in magnetostatics by the individual switching events. The increase in dipolar energy is proportional to an effective field that stabilizes the magnetization configuration of state 3. This stabilization field decreases with lower M_{SL}/M_{SH} ratios as demonstrated by the dependence of $\Delta\mu_0 H = |\mu_0 H_{1-2} - \mu_0 H_{3-4}|$ on M_{SL}/M_{SH} as shown in the inset of Fig. 9. The system approximates an array of magnetically isolated stripes when reducing M_{SL}/M_{SH}. Nevertheless, there still exists a value $\Delta\mu_0 H > 0$ for $M_{SL}/M_{SH} = 0$ that is due to dipolar interactions between the stripes.[29,30]

V. CONCLUSIONS

The influences of dipolar fields on the magnetization reversal of stripe arrays with alternating saturation magnetization values were modeled analytically and compared to experimental results. The model accurately predicts most of the magnetization reversal along and perpendicular to the stripe axis, its dependence on parameters like array and stripe size, and the effects of varying the ratio M_{SL}/M_{SH} between the saturation magnetization values of the individual stripes. It is shown that a lateral exchange-spring effect exists only in a certain range of size parameters and values of M_{SL}/M_{SH}. For M_{SL}/M_{SH} close to 1 in micrometer-sized

stripe arrays, the external boundary of the array is dominant and the magnetic properties are comparable to the properties of an unstructured element without exchange-spring behavior. The effect of the external boundary can be reduced by either increasing the size of the array or a reduction of M_{SL}/M_{SH}. A smaller M_{SL}/M_{SH} value lowers the influence of the outer interface and the magnetization reversal is governed by the internal interface between the stripes, which is a necessary condition to form an exchange-spring system. The exchange-spring effect, however, vanishes for M_{SL}/M_{SH} approaching zero, since the exchange coupling also reduces. The model can be used to predict the occurrence of an exchange-spring effect for different sample parameters. This can be calculated very effectively using the analytical model based on fundamental micromagnetic principles, as proposed in this paper. The understanding of the interactions between the dipolar energy and the lateral exchange-spring effect given by this paper opens the way to create systems for fascinating studies on exchange coupled systems, both lateral systems and multilayers in the out-of-plane direction.

ACKNOWLEDGMENTS

The authors thank N. Michalke and R. Mattheis from IPHT-Jena for the film deposition, T. Strache for performing the ion irradiation, A. Banholzer for *e*-beam lithography, C. Patschureck and A. Neudert for fruitful discussions, and the German Science Foundation (DFG) for funding the project through Grant No. DFG-Mc 9/7.

*n.martin@hzdr.de

[1] S. Blomeier, B. Hillebrands, B. Reuscher, A. Brodyanski, M. Kopnarski, and R. L. Stamps, Phys. Rev. B **77**, 094405 (2008).
[2] S. Neusser and D. Grundler, Adv. Mater. **21**, 2927 (2009).
[3] V. V. Kruglyak, P. S. Keatley, A. Neudert, R. J. Hicken, J. R. Childress, and J. A. Katine, Phys. Rev. Lett. **104**, 027201 (2010).
[4] J. McCord, Y. Henry, T. Hauet, F. Montaigne, E. E. Fullerton, and S. Mangin, Phys. Rev. B **78**, 094417 (2008).
[5] R. Hertel, J. Magn. Magn. Mater. **249**, 251 (2002).
[6] S. Goolaup, N. Singh, A. O. Adeyeye, V. Ng, and M. B. Jalil, Eur. Phys. J. B **44**, 259 (2005).
[7] A. Aharoni, J. Appl. Phys. **82**, 1281 (1997).
[8] J. Slonczewski, B. Petek, and B. Argyle, IEEE Trans. Magn. **24**, 2045 (1988).
[9] J. Fassbender and J. McCord, J. Magn. Magn. Mater. **320**, 579 (2008).
[10] J. McCord, L. Schultz, and J. Fassbender, Adv. Mater. **20**, 2090 (2008).
[11] E. E. Fullerton, J. S. Jiang, M. Grimsditch, C. H. Sowers, and S. D. Bader, Phys. Rev. B **58**, 12193 (1998).
[12] J. Fassbender, J. von Borany, A. Mücklich, K. Potzger, W. Möller, J. McCord, L. Schultz, and R. Mattheis, Phys. Rev. B **73**, 184410 (2006).
[13] J. Ziegler [http://www.srim.org/].
[14] C. Kittel, Rev. Mod. Phys. **21**, 541 (1949).
[15] L. Néel, C. R. Hebd. Seances Acad. Sci. **241**, 553 (1955).
[16] S. Middlehoek, J. Appl. Phys. **34**, 1054 (1963).
[17] W. Rave and A. Hubert, IEEE Trans. Magn. **36**, 3886 (2000).
[18] A. Hubert, Phys. Status Solidi B **38**, 699 (1970).
[19] A. Aharoni, J. Appl. Phys. **83**, 3432 (1998).
[20] C. Kooy and U. Enz, Philips Res. Rep. **15**, 7 (1960).
[21] Z. Malek and V. Kambersky, Czech. J. Phys. **8**, 416 (1958).
[22] W. Wernsdorfer, B. Doudin, D. Mailly, K. Hasselbach, A. Benoit, J. Meier, J. P. Ansermet, and B. Barbara, Phys. Rev. Lett. **77**, 1873 (1996).
[23] A. Thiaville, J. Magn. Magn. Mater. **182**, 5 (1998).
[24] B. Y. Wong and D. E. Laughlin, J. Appl. Phys. **79**, 6455 (1996).
[25] T. Trunk, M. Redjdal, A. Kákay, M. F. Ruane, and F. B. Humphrey, J. Appl. Phys. **89**, 7606 (2001).
[26] W. C. Uhlig and J. Unguris, J. Appl. Phys. **99**, 08G302 (2006).
[27] A. Hubert and R. Schäfer, *Magnetic Domains* (Springer, Berlin, 2009), pp. 23–49.
[28] A. Aharoni, L. Pust, and M. Kief, J. Appl. Phys. **87**, 6564 (2000).
[29] M. Wolf, C. Patschureck, R. Schäfer, L. Schultz, and J. McCord, J. Magn. Magn. Mat. **323**, 1703 (2011).
[30] F. Zighem, T. Maurer, F. Ott, and G. Chaboussant, J. Appl. Phys. **109**, 013910 (2011).